PAPER

Check for updates

Simulation guided molecular design of hydrofluoroether solvent for high energy batteries†

Zhou Yu, ‡[ab] Zhangxing Shi,‡[ac] Sambasiva R. Bheemireddy, [ac] Ethan Kamphaus,[ab] Xingyi Lyu,[d] Mohammad Afsar Uddin, [aej] Zhiguang Li,[acg] Zhenzhen Yang,[ac] Tao Li,[adf] Jeffrey S. Moore, [aehi] Lu Zhang [*ac] and Lei Cheng*[ab]

Electrolyte design is critical for enabling next-generation batteries with higher energy densities. Hydrofluoroether (HFE) solvents have drawn a lot of attention as the electrolytes based on HFEs showed great promise to deliver highly desired properties, including high oxidative stability, ionic conductivity, as well as enhanced lithium metal compatibility. However, the solvation-property relationships and design principles for high-performance HFE solvents are still poorly understood. Herein, we proposed four novel asymmetric HFE designs by systematically varying polyether and fluorocarbon structural building blocks. By leveraging molecular dynamics (MD) modeling to analyze the solvation structures and predict the properties of the corresponding 1 M lithium bis(fluorosulfonyl)imide (LiTFSI) solutions, we downselected the most promising candidate based on high conductivity, solvation species distribution, and oxidative stability for extensive electrochemical characterizations. The formulated electrolyte demonstrated properties consistent with the predictions from the simulations and showed much-improved capacity retention as well as coulombic efficiency compared to the baseline electrolytes when cycled in lithium metal cells. This work exemplifies the construction of candidate electrolytes from building block functional moieties to engineer fundamental solvation structures for desired electrolyte properties and guide the discovery and rational design of new solvent materials.

[a] *Joint Center for Energy Storage Research, Argonne National Laboratory, Lemont, IL 60439, USA. E-mail: zhanglu77@gmail.com; chengl@ornl.gov*

[b] *Materials Science Division, Argonne National Laboratory, Lemont, IL 60439, USA*

[c] *Chemical Sciences and Engineering Division, Argonne National Laboratory, Lemont, IL 60439, USA*

[d] *Department of Chemistry and Biochemistry, Northern Illinois University, DeKalb, IL 60439, USA*

[e] *Department of Chemistry, University of Illinois at Urbana-Champaign, Urbana, IL 61801, USA*

[f] *X-ray Science Division, Argonne National Laboratory, Lemont, IL 60439, USA*

[g] *Indiana University–Purdue University Indianapolis, 723 West Michigan Street, Indianapolis, IN, 46202, USA*

[h] *Beckman Institute for Advanced Science and Technology, University of Illinois at Urbana-Champaign, Urbana, IL 61801, USA*

[i] *Department of Materials Science and Engineering, University of Illinois at Urbana-Champaign, Urbana, IL 61801, USA*

[j] *Instituto de Ciencia de Materiales de Madrid, Madrid 20849, Spain*

† Electronic supplementary information (ESI) available. See DOI: https://doi.org/10.1039/d3ta07670a

‡ Zhou Yu and Zhangxing Shi contributed equally to this work.

Increasing the energy density of batteries is highly desired as the world market of electric vehicles (EVs) proliferates. While lithium-ion batteries (LIBs) are still the most widely adopted energy storage solution for the application, the current chemistry is approaching its theoretical limits. Lithium metal anode has a theoretical capacity of 3860 mA h g^{-1} and the lowest reduction potential (*i.e.*, −3.04 V *vs.* SHE), making lithium metal battery (LMB) an attractive option with a doubled energy density compared to LIBs.[1] However, LMBs still have formidable challenges in battery stability and safety, both of which are closely related to lithium anode issues, including dendrite growth, dead lithium, *etc.*[2] While the widely used carbonate-based electrolytes do not mitigate those issues, electrolyte engineering is a critical approach for LMBs as certain formulations form a full passivation film on the Li surface, leading to enhanced solid electrolyte interphase (SEI) stability.

To this end, a broad range of parameters are available to tune electrolyte behavior or properties, including the composition of salt and solvent, concentration, temperature, solvent structure design, *etc.*[3–11] For example, salt-concentrated electrolytes have been shown to improve the performance of LMBs[6,12] as the high salt concentrations suppress the growth of dendrites through stabilizing the ionic concentration profiles,[13] and facilitate the formation of the stable anion-derived SEI.[14,15] The realized benefits of such electrolytes were attributed mainly to the unique solvation structure originating from the high concentration. The localized high-concentration electrolytes (LHCEs) have shown similar solvation structure features and performance enhancement without the high concentration of salts, which impairs conductivity and adds cost. However, the oxidative stability of the LHCEs is still limited.[8,9]

6294 | *J. Mater. Chem. A*, 2024, **12**, 6294–6301

This journal is © The Royal Society of Chemistry 2024

Novel solvents have also been heavily investigated, including variations of carbonates, nitriles, ethers, and sulfones.[11] Among them, ether-based electrolytes show the most reductive resistance due to the lack of reduction-sensitive double bonds. However, for the same reason, they also suffer limited oxidative stability.[16] Introducing fluorine to ether backbones is an effective approach to increasing oxidative stability. Recently, several electrolytes based on hydrofluoroether (HFE) solvents have shown promising properties, including high oxidative stability, fast ionic conductivity, and enhanced lithium metal compatibility.[7,8,17,18] For instance, fluorinated orthoformate, when used as a co-solvent in LMBs facilitates the formation of highly homogeneous monolithic SEI, suppressing Li dendrite growth.[17] Another synthesized fluorinated ether, DEG-FtriEG, demonstrates both high ionic conductivity (2.7×10^{-4} S cm^{-1}) and high oxidative stability (5.6 V).[8] A recently reported HFE solvent, fluorinated 1,4-dimethoxylbutane, exhibits surprisingly excellent compatibility with Li metal and outstanding LMB performance when used in a single solvent electrolyte of 1 M lithium bis(fluorosulfonyl)imide (LiFSI).[7] Despite the exciting progress and attempts to reveal an in-depth understanding of the solvation impact, systematic investigation of the effects of building block groups of fluorocarbons and polyethers on the solvation structure, ion dynamics, and battery performance is absent, and the solvation-property relationships of the electrolyte at a molecular level are elusive.

In this study, we adopted an asymmetric design and proposed a new family of HFE solvents by varying the lengths of fluorocarbon and polyether segments, as shown in Scheme 1. Unlike other reported HFE structures, the polyethers were introduced into fluorocarbons only on one side or asymmetrically, intentionally creating intramolecular dipole moments that could benefit the solvating capability of Li ions. The notation of those structures (F_xO_y with $x, y = 2, 3$) was defined using the numbers of fluorinated carbon and oxygen atoms incorporated. To accelerate the discovery process, density functional theory (DFT) calculations, *ab initio*, and classical molecular dynamics (AIMD/CMD) simulations were used to establish the *in silico* screening protocols toward key properties of electrolytes composing of 1 M LiTFSI in those HFE solvents. Specifically,
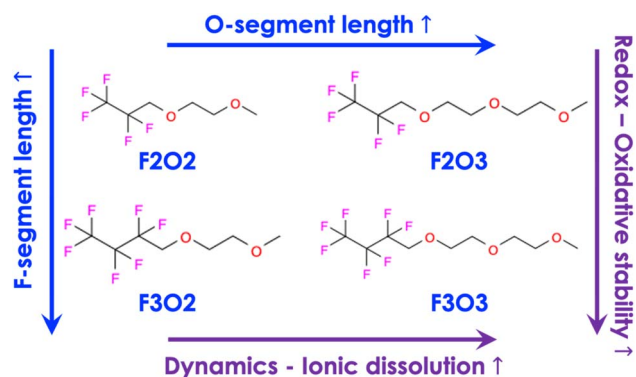
solvation structure, transport properties, redox stability of the electrolytes, and their reactivity with Li anode were investigated. The experimental characterizations were followed to validate the results. Based on this approach, the most promising candidate, F_2O_3, was selected for extensive battery performance characterization, showing improved cycling performance. The LMB cell using 1 M LiTFSI in F_2O_3 as the electrolyte with a metallic Li anode and an NMC622 cathode showed high average coulombic efficiency and excellent capacity retention for 100 cycles at a C/3 rate. This work highlights the adoption of *in silico* design protocols to accelerate the discovery loop of HFE solvents for LMBs through the understanding of the solvation-property relationship and further tailoring the chemical design to tune solvation structures.

Solvation structure

The solvation structure of electrolytes is closely related to their properties. Hence, we first characterize the solvation structures of 1 M LiTFSI in HFE solvents *via* MD simulations (simulation details are in ESI†). From the radial distribution function (RDF) analysis (Fig. S2†), we see that Li ions are coordinated mainly by O atoms in TFSI ions (O-TFSI) or solvent molecules (O-SOL), and the contribution from F atoms in solvent molecules (F-SOL) within the first solvation shell is very small (<3%). From the averaged coordination number analysis shown in Fig. 1a, as the polyether segment increases from F_2O_2 electrolyte to F_2O_3 electrolyte or from F_3O_2 electrolyte to F_3O_3 electrolyte, the coordination numbers (CNs) of O-TFSI decrease, and the CNs of O-SOL increase, while the total CNs (TOT) are similar for all solvents.

Time-averaged appearance frequency analysis of the CNs represented using 2D density maps (Fig. 1b–e) reveals more details on dominant solvation compositions. The figures show that the most common solvation structures in all four electrolytes have both O-TFSI and O-SOL coordination, but the exact numbers vary as the solvents change. In F_2O_2 and F_3O_2 electrolytes, the preferred Li ion coordination environments (identified by the high occurrence frequency areas, see color bar) consist of either 2 O-SOLs and 4 O-TFSIs or 4 O-SOLs and 2 O-TFSIs, with the former being more favorable. In F_2O_3 and F_3O_3 systems, the majority of Li ions are coordinated with 5 or 6 O-SOLs, while a small percentage are coordinated with a combination of 3 O-SOLs and 3 O-TFSIs. By further examining the coordination species (Fig. S3†), we observe that the coordinated Os in the solvation shell are from 1–2 solvent molecules and 2–3 TFSI ions in the F_2O_2 and F_3O_2 electrolytes. As the polyether chains increase in F_2O_3 and F_3O_3 electrolytes, the Li ions are more likely to be coordinated by either just two solvent molecules or two solvent molecules plus 1 TFSI ion. This observation is consistent with the more substantial chelating effect of the increased polyether length. The three most prominent and representative solvation structures in each electrolyte in MD simulations are shown in Fig. S4.†

The speciation of ions is further categorized based on their local solvation structure as free ion/solvent-separated ion pair (free/SSIP), contact ion pair (CIP), and aggregate (AGG), in
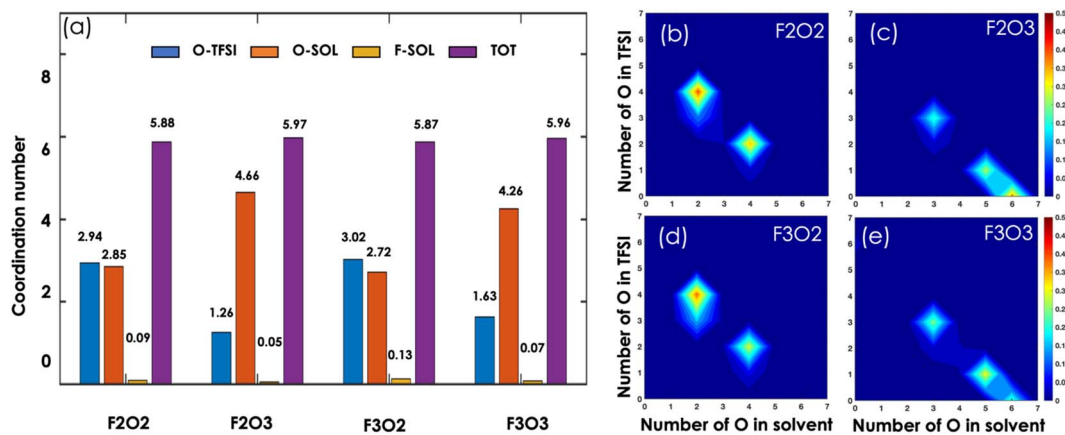
Scheme 1 Structures of novel fluorinated ethers with varied polyether and fluorocarbon segments that we investigated in this work.

This journal is © The Royal Society of Chemistry 2024

J. Mater. Chem. A, 2024, **12**, 6294–6301 | **6295**

Fig. 1 Solvation structure analysis of 1 M LiTFSI in F_2O_2, F_2O_3, F_3O_2, and F_3O_3 solvents. (a) Coordination number (CN) of Li ions with Os of TFSI ions (O-TFSI), Os of solvent molecules (O-SOL), and Fs of solvent molecules (F-SOL) in different electrolytes. The total CN is represented by TOT. (b–e) Time-averaged appearance frequency of the CNs of Li ions by Os in TFSI ions and solvent molecules in different electrolytes. The color bar represents the occurrence frequency.

which these ions are coordinated by zero, one, or more than one counterions, respectively.[19,20] From Fig. 2a, we can see more than 90% of Li ions form AGG in F_2O_2 and F_3O_2. As the polyether chain increases in length, the AGG formation is suppressed, and the fraction of free/SSIP and CIP increases. On the other hand, the increase of fluorinated moieties (F_3O_y vs. F_2O_y) seems to correlate with an increased AGG fraction. The speciations of 1 M LITFSI in F_2O_3 and F_3O_3 were also studied by Raman. The synthesis details of F_2O_3 and F_3O_3 were described in the ESI.† Previous literature studies have used Raman measurements of the TFSI breathing mode at peak positions around 740–750 cm^{-1} to characterize and quantify speciations in various electrolyte systems.[21] We fitted the peaks from our experiments (Fig. 2b) following the previous literature, assigning the free ion peak at 740 cm^{-1}, contact ion pair (CIP) peak at 745 cm^{-1}, and aggregate (AGG) peak at 750 cm^{-1} (ref. 14, 22 and 23) (details on spectral deconvolutions shown in Fig. S5†). The resulting percentages from the integrated Raman intensities are shown in Fig. 2c. The observation of more AGG in the F_3O_3 electrolyte than in the F_2O_3 electrolyte is qualitatively consistent with MD simulation, validating the effect of molecular design predicted by simulations.

Besides the well-studied local solvation structures, detailed analysis of the aggregates is necessary as the nanometric aggregate (n-AGG) has recently been observed in electrolytes for various battery chemistries, and these long-range structures inevitably influence ion transport, redox characteristics, and mechanics.[20] The aggregate structure analysis (Fig. S7†) shows that small ionic aggregates with several ions are the most common, while n-AGG with several tens of ions also exists in the electrolytes. The increase of polyether segments of those solvents correlates with the reduced sizes of n-AGG. Aggregate structures are more commonly observed in electrolytes with high salt concentrations where the systems are close to the solubility or precipitation limit. In the HFE solvents studied here, these limits are low because of the weaker solvation ability of HFE and strong solvent–solvent interactions resulting from the fluorous effect.[24–26] For example, a majority (>85%) of F atoms in solvent molecules are in close contact with at least another F atom of a different solvent molecule, as shown in Table S3 and Fig. S8.† Such solvent–solvent interactions limit the flexibility of solvents to coordinate freely with salt, contributing to the relatively low solubility of salt in HFE.
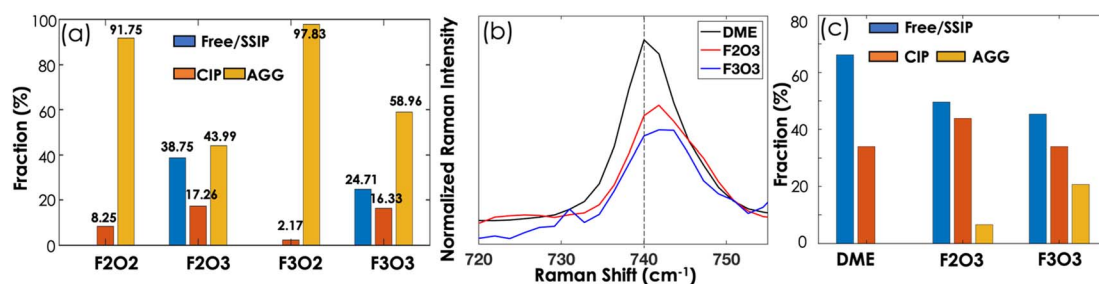

Fig. 2 (a) Fraction of ions in free ion/solvent-separated ion pair (free/SSIP), contact ion pair (CIP), and aggregate (AGG) solvation structure. (b) Raman spectral comparison of the TFSI breathing model region for solutions of 1 M LiTFSI in F_2O_3, F_3O_3 and DME solvents. The frequency of the free/SSIP TFSI model is indicated by a dashed line to guide the eyes. (c) Calculated percentage of the integrated Raman signal intensity in each electrolyte.

6296 | J. Mater. Chem. A, 2024, **12**, 6294–6301

This journal is © The Royal Society of Chemistry 2024

Dynamics properties

The second step of this *in silico* design is to estimate the dynamic properties of electrolytes, which are vital to battery performance. From the macroscopic standpoint, we calculated the self-diffusivity of cation, anion, and solvent and the ionic conductivity of the electrolyte. The results are reported in Table S4,† and the normalized results are shown in Fig. 3a. The calculation methods were introduced elsewhere.[27] We observe that as the size of solvent molecules increases, the self-diffusivities of ions and solvents decrease, which is consistent with the Stokes–Einstein relation that a larger solvent molecule slows the electrolyte dynamics. Increasing the polyether length correlates positively to the calculated ionic conductivity, as F_2O_3 and F_3O_3 electrolytes have higher conductivity compared to those of F_2O_2 and F_3O_2 electrolytes. The F_2O_3 electrolyte has a significantly higher conductivity, which is nearly three times the second-highest value of the F_3O_3 electrolyte. We note that the F_2O_2 electrolyte has the highest ion and solvent diffusivities but relatively low ionic conductivity. The strong correlation among species in the electrolytes leads to this highly nonideal behavior. From the microscopic standpoint, we quantify the dynamics of electrolytes by the lifetime of Li-TFSI ion pairs and the transport mechanism of ions. As shown in Fig. 3b, the lifetime of Li-TFSI ion pairs in different electrolytes is calculated by fitting the Li-TFSI association correlation function shown in Fig. S9 (see the ESI† for details). The longer polyethers reduce the lifetime of the Li-TFSI ion pair, which correlates negatively with the calculated ionic conductivity. Thus, the cation–anion association in CIP or AGG is responsible for the decreased ionic conductivity of the electrolytes.

Redox properties and SEI formation

Another important step is to estimate the redox characteristics of the electrolytes and how they affect SEI formation. The redox properties were first determined through the analysis of HOMO and LUMO energies from DFT calculations shown in Table S5.† It is clear that the fluorinated ethers have lower HOMO and LUMO levels as compared to a non-fluorinated ether solvent dimethoxyethane (DME). Lower HOMO corresponds to

improved oxidative stability, which is a known effect of fluorination. Lower LUMO indicates that the molecule is more readily reduced, presenting an opportunity to tune the solid electrolyte interphase (SEI) layer towards prolonged cycle life[28] and reduced interfacial resistance[29] through solvent formulation. The higher fraction of CIP and AGG in the fluorinated electrolytes (see Fig. 2) compared to the DME system (see Fig. S10†) also suggests lower LUMO energy levels of the TFSI ion affected by the coordinated Li ion[6] and a greater likelihood of reduction, which may promote an anion-derived SEI layer that is known to benefit SEI passivation.[28,29]

The interfacial reactions that initiate the formation of the SEI layer are studied *via* AIMD simulations of the electrolytes in contact with a Li metal anode. We perform simulations on DME, F_2O_3, and F_3O_3 electrolytes for comparison. The initial and final structures and the Bader charge analysis results of these simulations are reported in Fig. 4. In the 1 M LiTFSI in DME electrolyte, DME remains unreactive within the 10 ps of simulation time (Fig. 4a and c), which is consistent with the recent literature study.[30] Despite not being in direct contact with the Li surface, the LiTFSI salt reacts within the short simulation time. The reduction and decomposition of TFSI ion *via* N–S is observed at ∼4.50 ps, and 2 electrons transfer from the metallic Li electrode to the salt during the cleavage of N–S (Fig. 4c). As shown in Fig. 4b, the decomposition of F_2O_3 *via* C–F bond breaking occurs within 0.5 ps of simulation time, and the cleavage of the C–O bond is observed after 5 ps. The decomposition of TFSI ion *via* N–S, C–F, and S–O also occurs fairly early before 3 ps. The prominent charge transfer from the electrode to solvent and salt is shown in Fig. 4d. We note that the cleavage time of a certain type of bond may slightly change with different initial configurations. For example, in simulations where the salt species are in contact with the Li surface, salt and F_2O_3 decomposition also occur within 10 ps of simulation but at different times (see Fig. S11†). In the F_3O_3 system shown in Fig. S12,† the C–F bond of the HFE breaks within the initial 100 fs, and C–O bond breakage is observed within the first 0.5 ps for some species. The reduction is not limited to a single species but occurs for multiple HFEs throughout the trajectory. The overall amount of charge transferred to the solvent from the Li electrode is similar between the F_2O_3 and
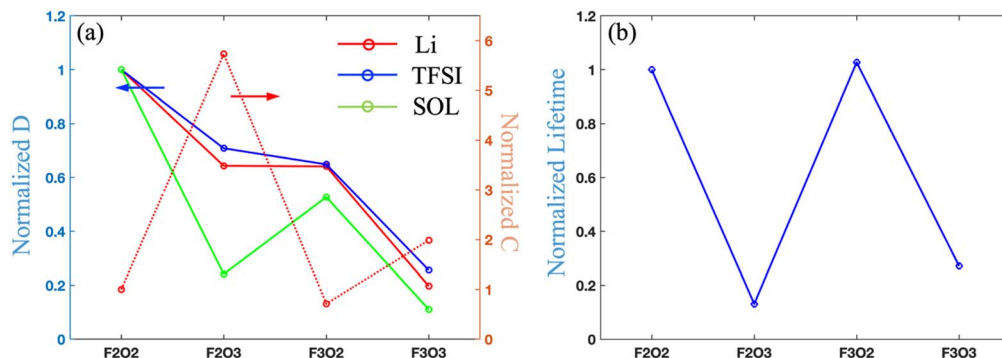

Fig. 3 (a) Self-diffusivity (*D*) of Li ion, TFSI ion, and solvent molecule and ionic conductivity (*C*); (b) lifetime of Li TFSI ion pair. All data is normalized by the F_2O_2 system and the exact data is summarized in Table S4.†

This journal is © The Royal Society of Chemistry 2024

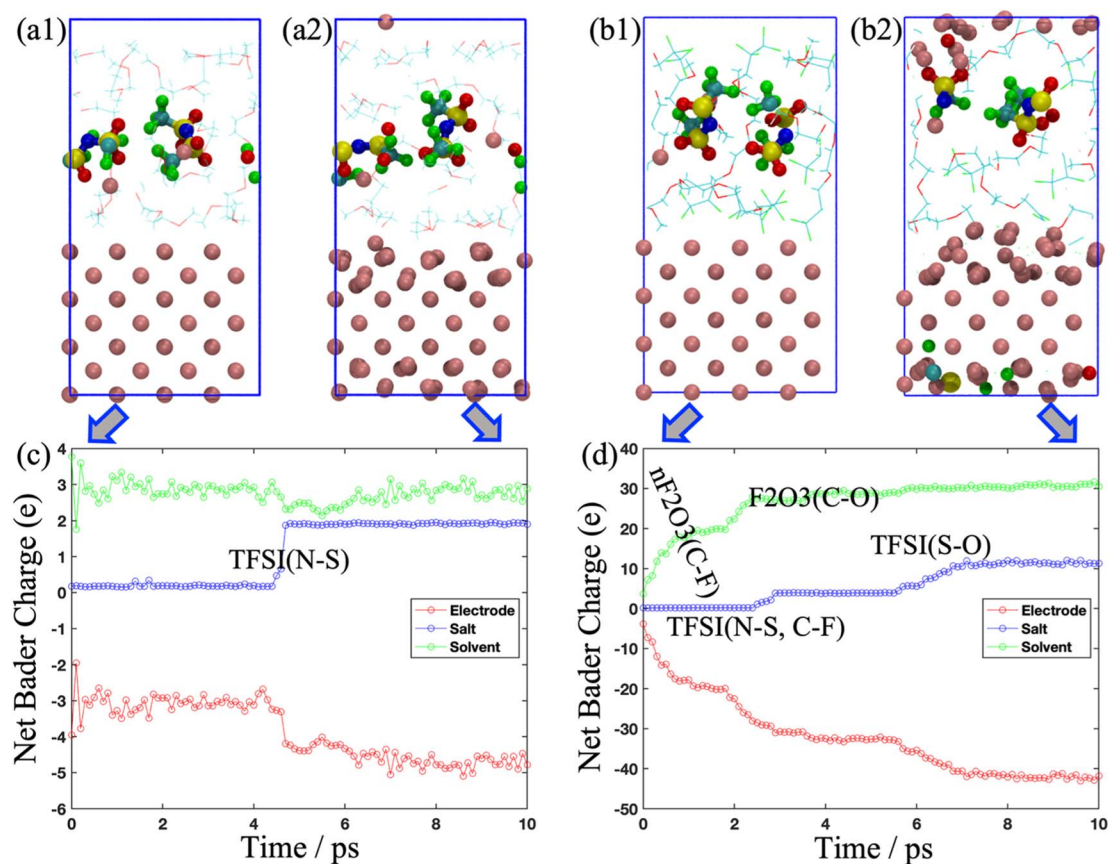*J. Mater. Chem. A*, 2024, **12**, 6294–6301 | **6297**

Fig. 4 The initial and final snapshots extracted from AIMD simulations with (a) DME as solvent or (b) F_2O_3 as solvent. LiTFSI locates in the middle of the electrolyte in the initial configuration. Pink, blue, yellow, red, cyan, and green balls denote Li, N, S, O, C, and F, respectively. The solvent molecules are depicted as wireframe. Net Bader charges of components in systems with (c) DME as solvent or (d) F_2O_3 as solvent.

the F_3O_3 case but occurs on a faster time scale for F_3O_3. Despite the similarities in charge transfer and reactions with the HFE, the TFSI molecules do not undergo a reduction in the F_3O_3 case. The overall charge of TFSI molecules remains close to neutral, and the bonds/structure of the molecule is intact. This indicates that the reduction of F_3O_3 is more favorable than the TFSI and the F_2O_3. Nevertheless, we highlight that the decomposition of newly synthesized fluorinated ether is more facile than DME due to the strong electron-withdrawing effect of the F functional group,[31] likely leading to fluorine-rich SEI layers that can be beneficial to stabilizing Li metal anodes.

Battery performance validation

Based on the simulation results of solvation structures, dynamic properties, redox characteristics, and associated possible SEI involvements, we identify the F_2O_3 electrolyte as the most promising candidate as it possesses balanced properties including high conductivity, high oxidative stability as well as feasible SEI reactivity. As expected, both F_2O_3 and F_3O_3 electrolytes show significantly improved oxidative stability compared to the DME electrolyte, as shown in Fig. 5. In the linear sweep voltammetry (LSV) tests (Fig. S13†), both electrolytes postpone the decomposing currents until above 5 V *vs.* Li/Li$^+$, while the DME electrolyte exhibits increased decomposition

at around 4.3 V *vs.* Li/Li$^+$. While F_2O_3 and F_3O_3 electrolytes start to decompose at the same potential, the F_3O_3 electrolyte has a much lower decomposition current, indicating its better oxidative stability. Interestingly, despite the structural similarity, the F_2O_3 electrolyte exhibits a significantly higher ionic conductivity of 1.81 mS cm^{-1} from the electrochemical impedance spectroscopy (EIS) measurements (Fig. S14†) compared to that of the F_3O_3 electrolyte at 0.76 mS cm^{-1}. These results agree well with the predicted values (see Tables S4 and S5†).

To further demonstrate the impact on cycling performance, those electrolytes undergo extensive electrochemical evaluations in Li metal cells using a LiNi$_{0.6}$Mn$_{0.2}$Co$_{0.2}$O$_2$ (NMC622) cathode. Fig. S15† summarizes the capacity retention and coulombic efficiency (CE) profiles of cells using an F_2O_3-based electrolyte (1 M LiTFSI in F_2O_3), an F_3O_3-based electrolyte (1 M LiTFSI in F_3O_3), a standard carbonate-based electrolyte (1.2 M LiPF$_6$ in EC/EMC = 3/7, plus 2 wt% vinylene carbonates, Gen 2–2% VC), as well as a DME electrolyte (1 M LiTFSI in DME). The 2032-type stainless steel coin cells used for evaluation consist of a lithium metal anode, a microporous polypropylene separator (Celgard 2325), an NMC622 cathode, and 25 μL of electrolyte. Details regarding cell assembly and cycling parameters can be found in the ESI.† The cells were subjected to three formation cycles at a C/10 rate followed by 100 cycles at a C/3 rate between

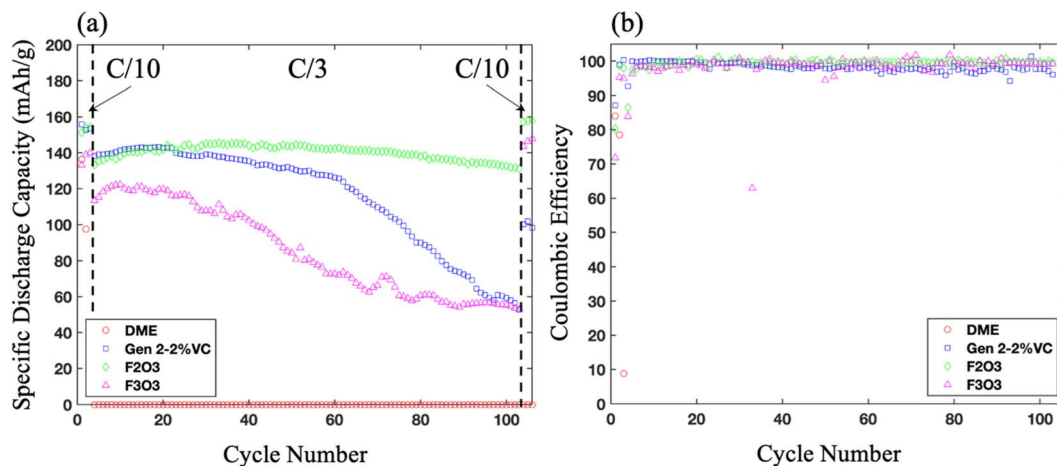**6298** | *J. Mater. Chem. A*, 2024, **12**, 6294–6301

This journal is © The Royal Society of Chemistry 2024

Fig. 5 (a) Discharge capacity and (b) coulombic efficiency profiles of as a function of cycle number for cells containing 1 M LiTFSI DME/F_2O_3/F_3O_3 electrolytes and 1 M LiPF$_6$ in EC/EMC (3/7) and 2% vinylene carbonate.

3.0 and 4.2 V. The DME cell shows very poor cycling as the capacity drops to nearly 0 within 4 cycles, possibly due to the cathode–electrolyte incompatibility. The Gen 2–2% VC cell shows better capacity retention, but only 38% capacity remains after 100 cycles. While the capacity retention of the F_3O_3 cell is even worse, the F_2O_3 cell shows a much-improved capacity retention with no obvious decay over 100 cycles. As for the CE profiles, DME cell drops from 80% to 0 within 4 cycles, while the Gen 2–2% VC, F_2O_3, and F_3O_3 cells show comparable values. F_2O_3 cell outperforms with a more stable profile and an average CE of 99.44%. Fig. S15† compiles the voltage–capacity profiles of those cells over 100 cycles. The DME cell shows decent charge–discharge curves for the first cycle but quickly fails on the second charge, suggesting severe decomposing reactions of DME when the cathode potential is raised. Both Gen 2–2% VC and F_3O_3 cells demonstrate increased overpotential as capacity drops over cycling. Only F_2O_3 cell exhibits low and stable overpotential over 100 cycles. The results suggest that besides the high conductivity, a stable SEI may form from the F_2O_3 electrolyte, evidenced by the limited overpotential increase and stable capacity retention.

To understand the SEI evolution, the cycled Li metal electrodes are investigated using X-ray photoelectron spectroscopy (XPS). Fig. 6 shows the F 1s, O 1s, and C 1s spectra of the cycled Li metal electrodes after 100 cycles. In the F 1s spectra, the electrode cycled with DME electrolyte exhibits an overwhelming LiF peak along with a LiTFSI peak. While inorganic LiF is known to strengthen the SEI layer, given DME mainly suffers severe decomposing on the cathode surface during high voltage cycling, the SEI on cycled Li metal surface may not provide enough justifications regarding the cell performance. On the other hand, both F_2O_3 and F_3O_3 electrodes show a LiF peak as well as a –(CF$_3$)-moiety peak, suggesting both solvents promote the CF composition during the SEI formation process. A similar observation is also found in the C 1s spectra. F_2O_3 and F_3O_3 electrodes show additional C–F peaks than the DME electrode. Interestingly, F_2O_3 exhibits only a –(CF$_3$)-moiety peak, and F_3O_3 shows both a –(CF$_3$)-peak and a –(CF$_2$)-peak. Considering

–(CF$_2$)- should most likely come from HFE solvents, F_3O_3 may suffer from more severe solvent decomposition, contributing to more irreversible capacity loss and corresponding deleterious cycling performance. Those observations are consistent with simulation results that the fluorinated ethers are more likely to participate in SEI formation, leading to F-rich components. However, an excess amount of solvent decomposition may not always benefit the SEI stability as well as cycling performance.

In this work, based on a new family of asymmetric HFE solvents, an *in silico* screening protocol was established to accelerate the discovery of HFE solvents through the understanding of the solvation-property relationship, predicting dynamics, redox properties, and possible roles in SEI formations. Analysis of simulation results reveals that the solvation structures of these HFE solvents are highly dependent on the choices of building segments, such as polyethers and fluorocarbons. For instance, HFEs with longer polyether chains are more likely to appear in the first solvation shell around Li ion with decreased number of coordinated TFSI ions and suppress the formation of ionic aggregates. Although the effect of the fluorocarbons on the solution structure is not as significant, increasing the fluorocarbons does impair the solvation effects of solvent molecules and benefits the formation of ionic aggregates. The selected F_2O_3 electrolyte exhibits a unique solvation structure featuring small dispersive aggregates composed of polyethers in the interstitial space of a percolated network composed of fluorocarbon segments.

By analyzing the solution structures, we then predicted the dynamic and redox properties of the HFE electrolytes. Consistent with solvation structure analysis, electrolytes with longer polyether chains are associated with higher ionic conductivities and shorter lifetimes of ion pairs due to the higher fraction of SSIP and weaker binding between ions, respectively. On the other hand, a higher fraction of CIP and AGG is related to the introduced fluorocarbons, which may benefit the formation of the anion-derived SEI layer. Furthermore, the interfacial reaction during the formation of the SEI layer is elucidated by the AIMD simulation and XPS experiments. We found the decomposition
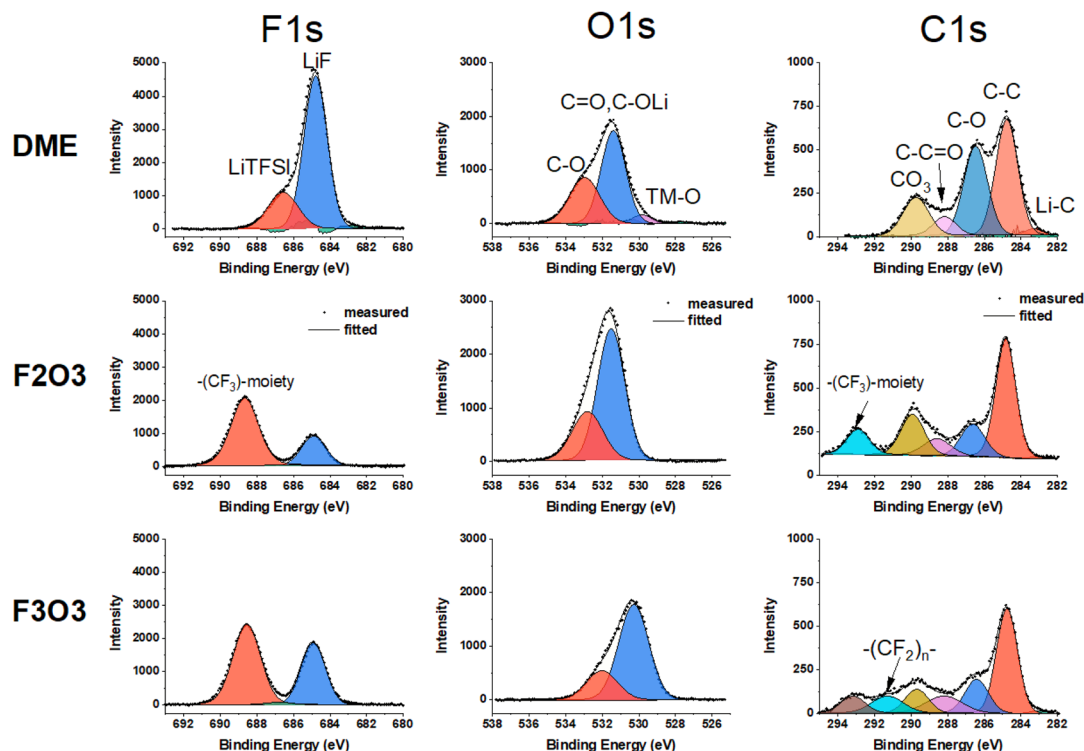
This journal is © The Royal Society of Chemistry 2024

J. Mater. Chem. A, 2024, **12**, 6294–6301 | **6299**

Fig. 6 F 1s, O 1s, and C 1s XPS spectra of the Li metal electrodes after 100 cycles.

of HFEs is much faster than that of DME, which contributes to the formation of fluorine-based SEI layers. Those results were verified *via* experimental evaluations of those HFE electrolytes. The electrolyte containing F_2O_3 indeed shows the highest conductivity, excellent oxidative stability, high ionic conductivity, and superb cycling performance in Li/NMC622 cells.

By adopting an *in silico* screening protocol, we demonstrated a simulation-guided development cycle for new HFE solvents through the understanding of the solvation-property relationship, predicting dynamic, redox properties, and possible roles in SEI formations. As predicted, the F_2O_3 solvent demonstrated much-improved dynamics, including high solubility of LiTFSI, much-enhanced conductivity, as well as excellent redox properties, such as improved oxidative stability, benefiting the SEI *via* solvent participation, collectively contributing to the superb cycling performance in Li/NMC622 cells. This work exemplified a prolific approach of using simulations to correlate fundamental solvation events and desired properties to the chemical structures constructed from building block functional moieties to guide the discovery and rational design of new solvent materials.

Conflicts of interest

The authors declare no competing financial interest.

Acknowledgements

References

1 L. Trahey, F. R. Brushett, N. P. Balsara, G. Ceder, L. Cheng, Y.-M. Chiang, N. T. Hahn, B. J. Ingram, S. D. Minteer and J. S. Moore, Energy storage emerging: a perspective from the Joint Center for Energy Storage Research, *Proc. Natl. Acad. Sci. U. S. A.*, 2020, **117**(23), 12550–12557.

2 F. Ding, W. Xu, X. Chen, J. Zhang, M. H. Engelhard, Y. Zhang, B. R. Johnson, J. V. Crum, T. A. Blake and X. Liu, Effects of carbonate solvents and lithium salts on morphology and coulombic efficiency of lithium electrode, *J. Electrochem. Soc.*, 2013, **160**(10), A1894.

3 Z. Yu, Y. Cui and Z. Bao, Design Principles of Artificial Solid Electrolyte Interphases for Lithium-Metal Anodes, *Cell Rep. Phys. Sci.*, 2020, **1**(7), 100119.

4 T. F. Miller III, Z.-G. Wang, G. W. Coates and N. P. Balsara, Designing polymer electrolytes for safe and high capacity

6300 | *J. Mater. Chem. A*, 2024, **12**, 6294–6301

This journal is © The Royal Society of Chemistry 2024

rechargeable lithium batteries, *Acc. Chem. Res.*, 2017, **50**(3), 590–593.

5 T. Famprikis, P. Canepa, J. A. Dawson, M. S. Islam and C. Masquelier, Fundamentals of inorganic solid-state electrolytes for batteries, *Nat. Mater.*, 2019, **18**(12), 1278–1291.

6 Y. Yamada, J. Wang, S. Ko, E. Watanabe and A. Yamada, Advances and issues in developing salt-concentrated battery electrolytes, *Nat. Energy*, 2019, **4**(4), 269–280.

7 M.-Y. He, C.-G. Luo, H.-J. Yang, F.-C. Kong, Y.-L. Li, L. Deng, X.-Y. Zhang and K.-Y. Yang, Sources and a proposal for comprehensive exploitation of lithium brine deposits in the Qaidam Basin on the northern Tibetan Plateau, China: Evidence from Li isotopes, *Ore Geol. Rev.*, 2020, **117**, 103277.

8 C. V. Amanchukwu, Z. Yu, X. Kong, J. Qin, Y. Cui and Z. Bao, A new class of ionically conducting fluorinated ether electrolytes with high electrochemical stability, *J. Am. Chem. Soc.*, 2020, **142**(16), 7393–7403.

9 S. Chen, J. Zheng, D. Mei, K. S. Han, M. H. Engelhard, W. Zhao, W. Xu, J. Liu and J. G. Zhang, High-voltage lithium-metal batteries enabled by localized high-concentration electrolytes, *Adv. Mater.*, 2018, **30**(21), 1706102.

10 N. Piao, X. Ji, H. Xu, X. Fan, L. Chen, S. Liu, M. N. Garaga, S. G. Greenbaum, L. Wang and C. Wang, Countersolvent Electrolytes for Lithium-Metal Batteries, *Adv. Energy Mater.*, 2020, **10**(10), 1903568.

11 K. Xu, Electrolytes and interphases in Li-ion batteries and beyond, *Chem. Rev.*, 2014, **114**(23), 11503–11618.

12 M. Li, C. Wang, Z. Chen, K. Xu and J. Lu, New concepts in electrolytes, *Chem. Rev.*, 2020, **120**(14), 6783–6819.

13 C. Brissot, M. Rosso, J.-N. Chazalviel and S. Lascaud, Dendritic growth mechanisms in lithium/polymer cells, *J. Power Sources*, 1999, **81**, 925–929.

14 Y. Yamada, K. Furukawa, K. Sodeyama, K. Kikuchi, M. Yaegashi, Y. Tateyama and A. Yamada, Unusual stability of acetonitrile-based superconcentrated electrolytes for fast-charging lithium-ion batteries, *J. Am. Chem. Soc.*, 2014, **136**(13), 5039–5046.

15 Y. Yamada, K. Usui, C. H. Chiang, K. Kikuchi, K. Furukawa and A. Yamada, General observation of lithium intercalation into graphite in ethylene-carbonate-free superconcentrated electrolytes, *ACS Appl. Mater. Interfaces*, 2014, **6**(14), 10892–10899.

16 S. Jiao, X. Ren, R. Cao, M. H. Engelhard, Y. Liu, D. Hu, D. Mei, J. Zheng, W. Zhao and Q. Li, Stable cycling of high-voltage lithium metal batteries in ether electrolytes, *Nat. Energy*, 2018, **3**(9), 739–746.

17 X. Cao, X. Ren, L. Zou, M. H. Engelhard, W. Huang, H. Wang, B. E. Matthews, H. Lee, C. Niu and B. W. Arey, Monolithic solid–electrolyte interphases formed in fluorinated orthoformate-based electrolytes minimize Li depletion and pulverization, *Nat. Energy*, 2019, **4**(9), 796–805.

18 L. Suo, W. Xue, M. Gobet, S. G. Greenbaum, C. Wang, Y. Chen, W. Yang, Y. Li and J. Li, Fluorine-donating electrolytes enable highly reversible 5-V-class Li metal

batteries, *Proc. Natl. Acad. Sci. U. S. A.*, 2018, **115**(6), 1156–1161.

19 W. A. Henderson, Glyme-lithium salt phase behavior, *J. Phys. Chem. B*, 2006, **110**(26), 13177–13183.

20 Z. Yu, N. P. Balsara, O. Borodin, A. A. Gewirth, N. T. Hahn, E. J. Maginn, K. A. Persson, V. Srinivasan, M. F. Toney and K. Xu, Beyond Local Solvation Structure: Nanometric Aggregates in Battery Electrolytes and Their Effect on Electrolyte Properties, *ACS Energy Lett.*, 2021, **7**, 461–470.

21 L. Suo, O. Borodin, T. Gao, M. Olguin, J. Ho, X. Fan, C. Luo, C. Wang and K. Xu, "Water-in-salt" electrolyte enables high-voltage aqueous lithium-ion chemistries, *Science*, 2015, **350**(6263), 938–943.

22 L. Suo, D. Oh, Y. Lin, Z. Zhuo, O. Borodin, T. Gao, F. Wang, A. Kushima, Z. Wang and H.-C. Kim, How solid-electrolyte interphase forms in aqueous electrolytes, *J. Am. Chem. Soc.*, 2017, **139**(51), 18670–18680.

23 D. W. McOwen, D. M. Seo, O. Borodin, J. Vatamanu, P. D. Boyle and W. A. Henderson, Concentrated electrolytes: decrypting electrolyte properties and reassessing Al corrosion mechanisms, *Energy Environ. Sci.*, 2014, **7**(1), 416–426.

24 Q. Sun, Z. Cao, Z. Ma, J. Zhang, H. Cheng, X. Guo, G.-T. Park, Q. Li, E. Xie and L. Cavallo, Dipole–Dipole Interaction Induced Electrolyte Interfacial Model To Stabilize Antimony Anode for High-Safety Lithium-Ion Batteries, *ACS Energy Lett.*, 2022, **7**(10), 3545–3556.

25 Y. Wang, Z. Cao, Z. Ma, G. Liu, H. Cheng, Y. Zou, L. Cavallo, Q. Li and J. Ming, Weak Solvent–Solvent Interaction Enables High Stability of Battery Electrolyte, *ACS Energy Lett.*, 2023, **8**(3), 1477–1484.

26 H. Liang, Z. Ma, Y. Wang, F. Zhao, L. Cao, L. Cavallo, Q. Li and J. Ming, Solvent–Solvent Interaction Mediated Lithium-Ion (De) intercalation Chemistry in Propylene Carbonate Based Electrolytes for Lithium–Sulfur Batteries, *ACS Nano*, 2023, **17**(18), 18062–18073.

27 E. J. Maginn, R. A. Messerly, D. J. Carlson, D. R. Roe and J. R. Elliot, Best practices for computing transport properties 1. Self-diffusivity and viscosity from equilibrium molecular dynamics [article v1.0], *Living Journal of Computational Molecular Science*, 2019, **1**(1), 6324.

28 H. Wang, W. Huang, Z. Yu, W. Huang, R. Xu, Z. Zhang, Z. Bao and Y. Cui, Efficient lithium metal cycling over a wide range of pressures from an anion-derived solid-electrolyte interphase framework, *ACS Energy Lett.*, 2021, **6**(2), 816–825.

29 R. Petibon, C. Aiken, L. Ma, D. Xiong and J. Dahn, The use of ethyl acetate as a sole solvent in highly concentrated electrolyte for Li-ion batteries, *Electrochim. Acta*, 2015, **154**, 287–293.

30 L. E. Camacho-Forero, T. W. Smith and P. B. Balbuena, Effects of high and low salt concentration in electrolytes at lithium–metal anode surfaces, *J. Phys. Chem. C*, 2017, **121**(1), 182–194.

31 X. Chen and Q. Zhang, Atomic Insights into the Fundamental Interactions in Lithium Battery Electrolytes, *Acc. Chem. Res.*, 2020, **53**(9), 1992–2002.

This journal is © The Royal Society of Chemistry 2024

J. Mater. Chem. A, 2024, **12**, 6294–6301 | **6301**